Dipolar effects on soliton dynamics on a discrete ferromagnetic chain

Jean-Pierre Nguenang,[1,2,3,*] Aurelien Jiotsa Kenfack,[1] and Timoléon Créprin Kofané[1]

[1]*Laboratoire de Mécanique, Faculté des Sciences, Université de Yaoundé I, B.P. 812, Yaoundé, Cameroon*

[2]*Condensed Matter Laboratory, Department of Physics, Faculty of Science, University of Douala, P.O. Box 24157, Douala, Cameroon*

[3]*The Abdus Salam International Centre for Theoretical Physics, P.O. Box 506, Strada Costiera, II-34014 Trieste, Italy*

The contributions of dipole-dipole interactions to the dynamics of solitons on a one-dimensional discrete easy-plane Heisenberg ferromagnet, in which the biquadratic exchange interactions are taken into account in addition to the Zeeman energy, the uniaxial anisotropy, and the exchange energy, are studied numerically. The results of a numerical simulation of the dynamics of a single soliton, as well as collision between a soliton-antisoliton pair, indicated that the energy-velocity curves for the solitons in the ferromagnetic chain present the signature of five different branches corresponding to different types of nonlinear elementary excitations in the chain.

PACS number(s): 42.65.Tg, 45.05.+x, 45.10.−b, 05.10.−a

I. INTRODUCTION

Many problems of mathematical physics, condensed-matter physics, mechanics of solids or fluids, and biological structures lead to the consideration of nonlinear equations having variables that are all continuous, partially discrete, or all discrete. Soliton equations belong to a special class of these nonlinear equations [1].

In addition, the discreteness makes the properties of the system periodic [2], so that due to the interplay between the discreteness and nonlinearity, new types of nonlinear excitations, which are absent in continuum models, may be possible in the system. This direction is rather new because until recently the main interest was in systems with strong coupling limit between spins or atoms, where a continuum approximation is generally applied in the theoretical model, revealing soliton solutions [3]. However, the continuum approximation, and thereby following exact soliton solutions are in many cases highly idealized.

From fundamental physical interest, the idea of a discrete nature has considerably improved our understanding of the effect of discreteness on topological solitons [4–8] and nontopological solitons [9], classical thermodynamic properties [10–13], modulational instabilities [14–16], wave-collapse phenomena [17,18], intrinsic localized vibrational states [19–21], diffusion in discrete nonlinear dynamical systems [22], and self-induced gap solitons [23,24].

Discrete models are also of interest for practical applications, such as systems of coupled optical waveguides [14,16,25–29], models for energy transport in biophysical systems proposed by Davydov [30], discrete models of sheibe aggregations [31], electrical arrays [32–34], systems that model the dynamics of DNA [35–38], discrete reaction-diffusion models to study propagation failure in myocardial tissue [39,40], for myelineated axons [41], discrete soliton equations related to cellular automata [42], discrete quantum motors [43], and discrete easy-plane ferromagnetic chain [44–46]. In the latter context, further investigations concerning the dipolar interaction contributions to the general properties of soliton's motion, as well as its modified profile, have been carried out in Ref. [47] using the long wavelength approximation. In this case, dipolar interactions contribute to increase the critical magnetic field, the stability of the Sine-Gordon soliton, and also the soliton contribution to the specific heat [47].

Assuming that the Heisenberg model for describing magnetic phenomena is inherently discrete, with lattice spacing being a fundamental physical parameter, Wysin, Bishop, and Kumar (WBK) [45] studied the dynamics of a single soliton as well as the collisions between a soliton-antisoliton pair by numerical simulations, accounting for both the magnetic field B_e and the propagation velocity u of a soliton. WBK showed that the solitons are multibranched. More precisely, the dynamics of a single soliton can be classified into three different branches, while that of collisions between a soliton-antisoliton pair consists of four major branches.

In the present paper, using the ideas and formal approach of WBK, we investigate the dipolar interaction contributions on the dynamics of solitons of a discrete ferromagnetic chain.

The paper is organized as follows. In Sec. II, the model Hamiltonian is introduced and a set of coupled nonlinear differential-difference equations of spin dynamics is derived. In Sec. III, some numerical results on the creation of solitons in a classical easy-plane discrete ferromagnetic chain under weak dipolar interactions starting from an initial Sine-Gordon (SG) soliton are presented, and their stability under collision is verified. Section IV is devoted to the conclusion.

II. THE MODEL

A. Equations of motion

The model we deal with in this section is a chain of classical spin interacting both by short-range nearest-neighbor ferromagnetic interactions and long-range dipolar interactions. It is also subject to an anisotropic field perpendicular

*Email addresses: nguenang@yahoo.com, jpnguen@uycdc.uninet.cm

to the chain direction and an in-plane applied magnetic field. Hence, the following Hamiltonian describes it:

$$H = -J\sum_i \vec{S}_i \cdot \vec{S}_{i+1} - g\mu_B B_e \sum_i S_i^x + A\sum_i (S_i^z)^2$$

$$-\alpha J \sum_i (\vec{S}_i \cdot \vec{S}_{i+1})^2 + \frac{1}{2}(g\mu_B)^2$$

$$\times \sum_{ii'} \left[\frac{\vec{S}_i \cdot \vec{S}_{i'}}{r_{ii'}^3} - \frac{3(\vec{S}_i \cdot \vec{r}_{ii'})(\vec{S}_i \cdot \vec{r}_{ii'})}{r_{ii'}^3} \right], \quad (2.1)$$

where the sums run over the lattice sites separated by a distance a_0 apart along the z axis, and where $S_i^\delta (-\delta = x, y, z)$ is the δ component of the spin vectors on the ith site. The first term in the Hamiltonian (2.1) represents the Heisenberg exchange energy, where $J > 0$ is the short-range nearest-neighbor exchange coupling constant. The spin may also be placed in an external field (B_e) directed along the x axis leading to the second term representing the Zeeman energy, where the quantities g and μ_B are the Landég factor and the Bohr magneton, respectively.

The third term is the single ion uniaxial anisotropy energy due to the crystalline field. It constrains the spin to lie in a plane perpendicular to the chain axis. A is the uniaxial crystal-field anisotropy parameter.

The fourth term represents the biquadratic isotropic exchange interactions, which should be considered for a high-spin system, with $S \geq 1$ [48]. The parameter α measures the strength of the biquadratic exchange, in the classical approximation. Adler gave a discussion of these biquadratic exchange interactions through an extensive review of experimental results, which establish the importance of this term in a variety of compounds [49]. The necessity of including such a term goes back to Schrödinger, and Anderson gave its interpretation in terms of a superexchange mechanism [50]. Kapor and Skrinjar gave another interpretation of the biquadratic exchange interactions in terms of three-spin exchange interaction [51]. For a ferromagnetic ground state, the parameter α has to satisfy, for $S = 1$, $0 < \alpha < 1$ and for a spin with $S > 1$, the condition is $-2/[S(2S-3)] < \alpha < 2(S+1)/S^2$ [48].

The last term of Hamiltonian (1) is the dipole-dipole interaction energy between the magnetic moments of the constituent atoms, where $r_{ii'} = |\vec{r}_i - \vec{r}_{i'}|$ is the distance between two different magnetic sites i and i'. An important implica-

tion of this last term on the critical dynamics of the uniaxial ferromagnet has been elucidated using the renormalization group method [52]. In contrast with the short-range exchange interaction, the dipolar interaction is long ranged and thus dominates the asymptotic critical behavior of the ferromagnet [53]. These interactions also introduce an anisotropy of the spin fluctuations longitudinal and transverse to the wave vector.

At sufficiently low temperatures $T \ll (AJ)^{1/2}$, while neglecting quantum effects, i.e., $A/JS(S+1) \ll 4\pi^2$, the spins can be considered as classical vectors where their orientations are parametrized by the spherical coordinates as

$$\vec{S}_i = S[\cos(\theta_i)\cos(\varphi_i), \cos(\theta_i)\sin(\varphi_i), \sin(\theta_i)], \quad (2.2)$$

where $-\pi/2 \leq \theta_i \leq \pi/2$ is the excursion angle of magnetization from (S_i^x, S_i^y) plane, and $0 \leq \varphi_i \leq 2\pi$ represents the azimuthal angle of $\vec{S}_i$ in the same plane. S is the magnitude of $\vec{S}_i$ and the dynamics of these spins can be described by the undamped Bloch equation

$$\hbar \frac{d\vec{S}_i}{dt} = \vec{S}_i \times \vec{F}_i. \quad (2.3)$$

Then, using the following relation for the effective field:

$$\vec{F}_i = -\frac{\partial H}{\partial \vec{S}_i}. \quad (2.4)$$

It comes that

$$\vec{F}_i = J\vec{S}_{i+1}(1 + 2\alpha\vec{S}_i \cdot \vec{S}_{i+1}) + J\vec{S}_{i-1}(1 + 2\alpha\vec{S}_i \cdot \vec{S}_{i-1})$$

$$-2AS_i^z \vec{e}_z + g\mu_B B_e \vec{e}_x + \frac{1}{2}(g\mu_B)^2$$

$$\times \sum_{i'} \left[\frac{\vec{S}_{i'}}{r_{ii'}^3} - \frac{3(\vec{r}_{ii'})(\vec{S}_{i'} \cdot \vec{r}_{ii'})}{r_{ii'}^3} \right], \quad (2.5)$$

where $\vec{e}_x(\vec{e}_z)$ is the unit vector along the x axis (the z axis). $\vec{F}_i$ represents the effective field acting on each spin, while $\vec{S}_i \times \vec{F}_i$ represents the torque on the spin at the site i, respectively. So, replacing Eqs. (2.2) and (2.5) into Eq. (2.3), we obtain

$$\frac{d\varphi_i}{dt} = JS\tan(\theta_i)\{1 + 2\alpha S^2[\sin(\theta_i)\cos(\theta_{i+1})\cos(\varphi_{i+1} - \varphi_i) + \cos(\theta_i)\sin(\theta_{i+1})]\}[\cos(\theta_{i+1})\sin(\varphi_{i+1} - \varphi_i)$$

$$-\cot(\theta_i)\sin(\theta_{i+1})] + JS\tan(\theta_i)\{1 + 2\alpha S^2[\sin(\theta_i)\cos(\theta_{i-1})\cos(\varphi_{i-1} - \varphi_i) + \cos(\theta_i)\sin(\theta_{i-1})]\}[\cos(\theta_{i-1})$$

$$\times \sin(\varphi_{i-1} - \varphi_i) - \cot(\theta_i)\sin(\theta_{i-1})] + 2AS^2\sin(\theta_i) + g\mu_B B_e \tan(\theta_i)\cos(\varphi_i)$$

$$+ \frac{1}{2}(g\mu_B S)^2 \sum_{i'} \frac{\sin(\theta_{i'})}{r_{ii'}^3}\{[\cos(\theta_{i'})\sin(\varphi_{i'}) + \sin(\theta_{i'})][\cos(\varphi_{i'}) + \sin(\varphi_{i'})]\}, \quad (2.6)$$

$$\frac{d\theta_i}{dt}=JS\{1+2\alpha S^2[\sin(\theta_i)\cos(\theta_{i+1})\cos(\varphi_{i+1}-\varphi_i)+\cos(\theta_i)\sin(\theta_{i+1})]\}\cos(\theta_{i+1})\sin(\varphi_{i+1}-\varphi_i)$$

$$+JS\{1+2\alpha S^2[\sin(\theta_i)\cos(\theta_{i-1})\cos(\varphi_{i-1}-\varphi_i)+\cos(\theta_i)\sin(\theta_{i-1})]\}\cos(\theta_{i-1})\sin(\varphi_{i-1}-\varphi_i)-g\mu_B B_e\sin(\varphi_i)$$

$$+\frac{1}{2}(g\mu_B S)^2\sum_{i'}\left(\frac{\cos(\varphi_{i'})}{r_{ii'}^3}\{[\cos(\theta_{i'})\cos(\varphi_{i'})+\sin(\theta_{i'})][\cos(\varphi_{i'})+\sin(\varphi_{i'})]\}\right.$$

$$\left.-\frac{\sin(\varphi_{i'})}{r_{ii'}^3}[\cos(\theta_{i'})\sin(\varphi_{i'})+\sin(\theta_{i'})]\right). \tag{2.7}$$

The set of coupled nonlinear differential-difference equations (2.6) and (2.7) define the collective excitations for the in-plane angle φ_i and the out-of-plane θ_i. In the absence of the biquadratic exchange and dipolar interactions, Etrich *et al.* [54] have shown that in the discrete ferromagnetic spin chain there may occur two essentially different static in-plane soliton structures, one with its center located on a lattice site (central-spin configuration), and the other with its center located in the middle between the two neighboring lattice sites (central-bond configuration).

B. Influence of the dipolar interactions in the continuum approximation

Meanwhile the model under study is discrete, it is important to derive the continuum limit, because it allows establishing the analytical calculation of the influence of the dipolar interactions on some critical parameters, so that with further numerical computations, some comparison could be done. Attention is then focused on the study of widely spatially extended solutions where the variations in space and time are slow, which allow us to use the continuum limit approximation. Then we can obtain the following perturbed SG equation [47]:

$$\frac{\partial^2\varphi}{\partial\tau^2}-\frac{\partial^2\varphi}{\partial Z^2}+b\sin(\varphi)$$

$$=b_d\left[\cos(2\varphi)-\left(\sin(2\varphi)\frac{\partial^2\varphi}{\partial Z^2}+\left(\frac{\partial\varphi}{\partial Z}\right)^2\cos(2\varphi)\right)\right], \tag{2.8}$$

and

$$\theta=\varphi_\tau, \tag{2.9}$$

where the dimensionless quantities are

$$\tau=\frac{2ASt}{\hbar}, \quad Z=\left(\frac{2A}{J(1+2\alpha S^2)}\right)^{1/2}\frac{z}{a_0}, \tag{2.10}$$

$$b=\frac{g\mu_B B_e}{2AS}, \quad b_d=\frac{g\mu_B H_d}{2AS}, \tag{2.11}$$

and here $H_d=4\pi N_d(N/V)g\mu_B S$ is the demagnetizing field due to the dipolar interactions and N_d being the demagnetiz-

ing factor, and V is the volume in the case of a cubic sample, but here since we are studying a single spin chain, it stands for the chain length. In rescaling the dimensionless length variables Z, as given in Eq. (2.10), it appears as the term $J(1+2\alpha S^2)$. As shown by Ferrer [55], this term is the consequence of the renormalization of the exchange energy, which is the only effect of the biquadratic exchange energy in the sine-Gordon limit. Without the biquadratic exchange and dipole-dipole interactions, that is $b_d=0$, Mikeska has shown that the dynamics of solitons in a ferromagnetic spin chain is described by the SG equation [56]. In other words, the ferromagnetic solitary excitations are composed of a 2π kink in φ and a pulse in θ which has amplitude proportional to the soliton speed. Later, Kumar [57,58], Magyari and Thomas [59] have already attracted the attention on the validity limits of the SG approximation for the ferromagnetic domain walls. In the absence of dipolar interaction, a linear stability analysis of a static SG soliton profile shows that for the applied magnetic field $B_e\geqslant B_{ec}=2A/3$ instability occurs. For this critical value of the applied magnetic field, the corresponding critical value of the reduced magnetic field is $b_c(0)=\frac{1}{3}$ and $\mathbf{b}_c(0)-\mathbf{b}_c(\mathbf{u})\approx\mathbf{u}^{2/3}$, where u is the soliton velocity. Then the presence of dipolar interactions in the right-hand side of Eq. (2.8) leads to the new instability criterion [47],

$$b\geqslant\hat{b}_c=\frac{1}{3}+a_1 g(\pi) \tag{2.12}$$

and

$$\hat{b}_c(0)-\hat{b}_c(u)\approx\chi(u\pm u_0)^{2/3}, \tag{2.13}$$

where

$$a_1=\frac{H_d S}{B_e},$$

$$g(\pi)=\frac{1}{18}\left[10.1\pi^3+12\pi^2-\frac{15\pi}{2}+96\pi\ln(2)+48\right]\approx 36, \tag{2.14}$$

$$\tilde{u}_0=\frac{\tilde{c}_1 b_d}{\pi}, \quad \chi=\frac{6c_4}{c_2}\left(\frac{c_1}{8c_4}\right)^{2/3}, \tag{2.15}$$

$$\tilde{c}_1=\frac{8\pi}{b^{1/2}}, \quad c_2=6b_c^{1/2}, \quad c_4=\frac{4}{5}b_c^{1/2}, \quad c_1=\pi. \tag{2.16}$$

We can also calculate the soliton effective mass m^* for $b < \hat{b}_c$; for small velocities u, the stability analysis yields the energy $E(u)$ of the moving soliton as

$$E(u) = E(0) + \frac{1}{2} m^* u^2, \qquad (2.17)$$

with

$$m^* = \frac{b b_c A(\lambda)}{\hat{b}_c - b}. \qquad (2.18)$$

Here, $\lambda = 2AS/g\mu_B B_e$, and $\hat{b}_c$, which is the lowest value of b given in Eq. (2.12), is the new critical reduced field when the dipolar interactions are taken into account. $A(\lambda)$ is a positive constant for which expression is derived in the Appendix. Also keep in mind that b_c is the critical field in the absence of the dipolar interactions. For $b < \hat{b}_c$ and $E(u) - E_{SG}(0) \ll E_{SG}(0)$, the soliton is SG-like with effective mass given by Eq. (2.18). This branch, which has been referred to as branch I by WBK, terminates at a maximum velocity $u_m(b)$. The branch II is related to the soliton propagation for $E > E(u_m)$, where the velocity u decreases with increasing energy E, leading finally to a second static soliton with an energy higher than $E_{SG}(0)$ and with $\theta_m = \theta_0$ such

that $E(\theta_0)$ is the maximum energy for a soliton. Using the ansatz of Liebmann *et al.* [60], we have been able to calculate the field dependence of the energy of this second static soliton and the corresponding excursion angle θ_0 as

$$E = E_{SG}(0) \left(\frac{2}{3} + b \right) \left(\frac{1}{3} + \frac{2}{9b} \right)^{1/2}, \qquad (2.19)$$

$$\sin^2 \left(\frac{\theta_0}{2} \right) = \hat{b}_c - b. \qquad (2.20)$$

Then in this region the results obtained in Eqs. (2.19) and (2.20) are identical to those of Liebmann *et al.* [60]. We observe, however, that the only difference is that there is some kind of renormalization in Eq. (2.19) on the expression of the soliton rest energy $E_{SG}(0)$ given in Ref. [47]. Finally, for the other branches, the solitons are moving with a negative velocity (relative to SG). These regions correspond to an inverted parabola. The effective mass of the solitons is given by [45]

$$m^{**} = \left. \frac{\partial (L - E)/\partial \theta_m}{\partial^2 E/\partial \theta_m^2} \right|_{\theta_0}, \qquad (2.21)$$

where the negative expression of a Lagrangian is given by

$$L(\theta, \varphi) = \int dZ \left\{ \left[\frac{1}{2} (\theta_Z^2 + \varphi_Z^2) + \frac{\cos^2(\theta)}{2} - b \cos(\theta) \cos(\varphi) - \varphi_\tau \sin(\theta) \right] + b_d \cos(2\theta)[-\varphi_Z^2 \sin(2\varphi) + \sin(2\varphi)] \right\}. \qquad (2.22)$$

Here, Z and τ are defined in Eq. (2.10). From Eqs. (2.21) and (2.22), we obtain

$$m^{**} = \frac{2\pi b_d (b_c/b)^{1/2}}{\hat{b} - b} \quad \text{for} \quad b > \check{b}_c. \qquad (2.23)$$

and

$$m^{**} = -\frac{\pi b_d (b_c b)}{\hat{b}_c - b} \quad \text{for} \quad b < \check{b}_c. \qquad (2.24)$$

Moreover, in the absence of dipolar interactions, the numerical simulations of soliton dynamics on a discrete ferromagnetic chain, without any SG assumptions, performed by WBK have revealed a rich behavior such as the existence of a multibranched single-soliton excitation structure.

III. NUMERICAL RESULTS

In this section, we report our numerical results. In order to check the dynamics of a single soliton as well as collisions between a soliton-antisoliton pair, we solve numerically the set of coupled nonlinear differential-difference equations of

motion (2.6) and (2.7) with a fourth-order Runge-Kutta scheme, so that the continuum approximation is not assumed in the numerical scheme. The time step [typically 0.03 in units $(JS)^{-1}$] is chosen to preserve the total energy of the spin chain to an accuracy of about 0.01% during the complete run. In the numerical simulations, we consider a system involving N spins ranging between $N = 100$ and 200 spins with periodic boundary conditions at the two ends of the chain in the case of the collision, but for the propagation of a single SG soliton we include an offset of 2π at the end of the spin chain. The single SG soliton and pairs of SG soliton-antisoliton provide initial conditions here.

A. Single-soliton dynamics

In order to study soliton properties in the discrete lattice in presence of dipolar interactions, we investigate numerically the discrete-lattice time evolution of soliton configurations. Approximate initial solutions of Eqs. (2.6) and (2.7) are the SG solitons

$$\varphi_{SG} = 4 \arctan(\exp \gamma \sqrt{b}[Z - u_{SG}\tau]), \qquad (3.1)$$

$$\theta_{SG} = -2\gamma \sqrt{b} u_{SG} \, \text{sech}[\gamma \sqrt{b}(Z - u_{SG}\tau)], \qquad (3.2)$$
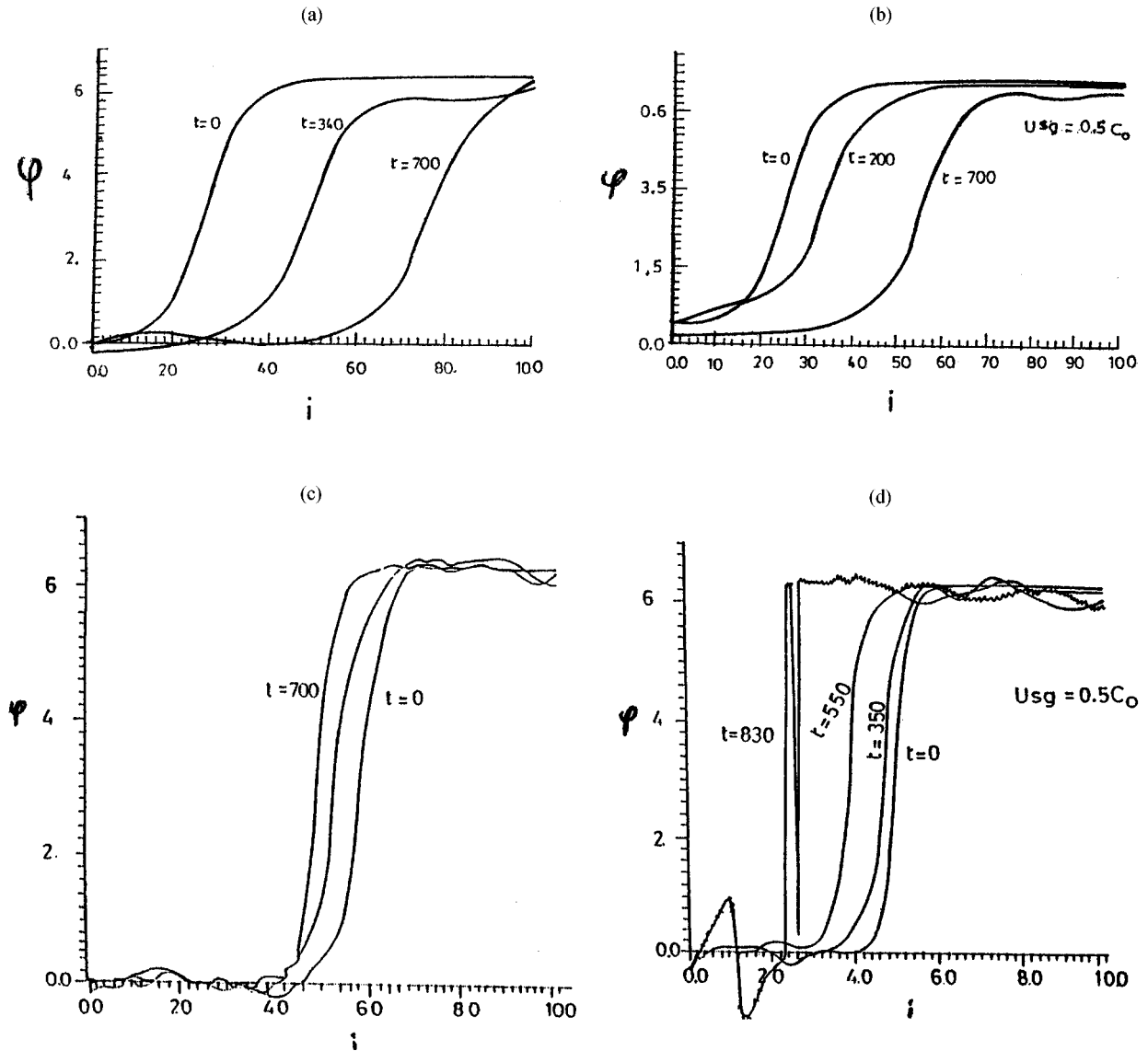
FIG. 1. Time development of an exact solution of the continuum equation of motion in a discrete Heisenberg chain. (a) Without dipolar interactions; (b) with dipolar interactions. Stability of a moving soliton, transition to a new configuration due to discreteness effects provided by increasing the magnetic field. (c) Without dipolar interactions; (d) with dipolar interactions.

where $\gamma = (1 - u_{SG}^2)^{-1/2}$ is the Lorentz contraction factor and u_{SG} is the velocity. Under this assumption, the degree of discreteness is controlled by the parameter $\gamma\sqrt{b}$. The smaller the $\gamma\sqrt{b}$, the better the continuum approximation. Let us introduce, as an example, the following set of parameters corresponding to the CsNiF$_3$ structure, namely [57]: $J = 23.6$ K, $A = 4.5$ K, and $S = 1$. Using the SG solitons [see Eqs. (3.1) and (3.2)] as initial conditions, we have verified their stability on the discrete lattice. Let the reduced magnetic field be chosen at the value of $b = 0.024$. The result of the numerical integration of the system of equations of motion (2.6) and (2.7) is shown in Figs. 1(a) and 1(b), respectively, where we observed that a soliton moving with a normalized constant speed $u_{SG} = 0.5C_0$ along the discrete chain and with a constant profile, where $C_0^2 = 2JSA(1 + 2\alpha S^2)a_0^2$ is stable when dipolar interactions are absent [see Fig. 1(a)] or present [see Fig. 1(b)]. In some figures, the cases of no

dipolar interactions are also shown for comparison. With increasing the reduced magnetic field up to a value of $b = 0.15$, and taking the normalized input velocity as $u_{SG} = 0.5C_0$, the degree of discreteness due to $\gamma\sqrt{b}$ increases and more magnons are generated with no dipolar interactions [see Fig. 1(c)]. Therefore the presence of magnons is evidently associated to the discreteness of the chain. More and more magnons are radiated in the presence of dipolar interactions, and the kink shape of the waves disappears progressively, such a situation can be seen in the sites $20 \leq i \leq 40$ of Fig. 1(d).

For further investigations of the dynamics of a single soliton in the presence of magnetic long-range interactions, we plot the observed average velocity u of the soliton as a function of the initial velocity u_{SG} for different magnetic fields. For a given magnetic field, the average velocity was obtained by averaging the instantaneous velocity of the soliton during
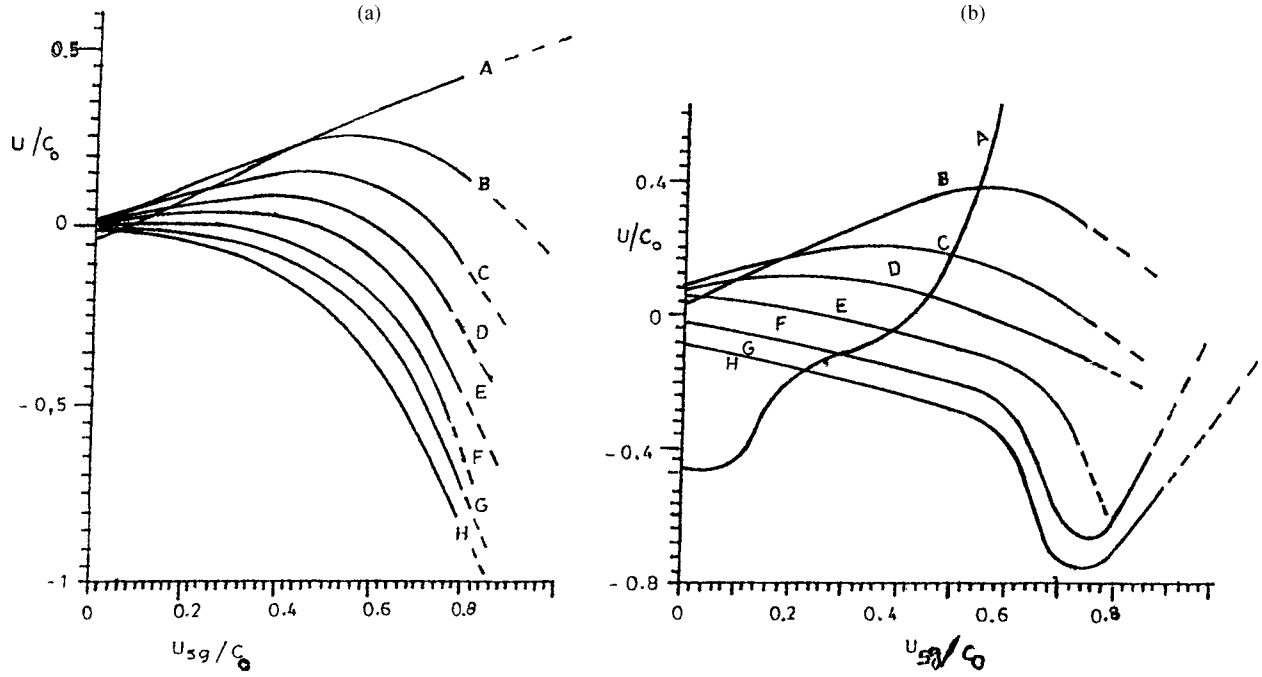
FIG. 2. (a) Mean kink effective velocity (u) against u_{SG} (Sine-Gordon kink velocity) when the dipole-dipole interactions are absent for different value of the reduced magnetic field b; $A=0$, $B=0.05$, $C=0.10$, $D=0.15$, $E=0.19$, $F=0.24$, $G=0.3$, $H=0.36$. (b) When the dipolar interactions are present for the same value of the magnetic field.

its propagation in the lattice. The results of our computations are shown in Figs. 2(a) and 2(b), respectively. At first, three results are mentioned:

(i) In Fig. 2(b), the curve A corresponds to the case of a soliton propagation when the magnetic field is nil. In this situation, some perturbing forces are induced in the system by the presence of the dipolar interactions. Their main effect is to constrain the resulting wave to propagate in the opposite direction to that of the initial condition with small velocities. Hence, in this case, the average velocity of the propagating kink begins by a negative value. It is only when the initial conditions attain a certain minimal velocity that the effective velocity of the resulting wave starts increasing. This can be understood in the sense that, when the initial condition is introduced in the chain with a certain initial momentum, the resulting wave is suddenly subject to competition between its momentum and the perturbing forces. Then the effective velocity of the resulting wave is negative and does not increase when the initial momentum of the kink is less than the perturbing forces. But when this initial momentum is greater or comparable to the perturbing forces, the effective velocity of the resulting wave increases. Therefore, due to the above-mentioned competition that leads to a permanent balance between the initial momentum of the initial condition and the perturbing forces, the effective velocity of the propagating kink while increasing exhibits a nonlinear behavior. This is different from the linear behavior observed in the curve A of Fig. 2(a), where dipolar interactions are absent.

(ii) In the presence of dipolar interactions, the average velocity u is always less than u_{SG}. In curves $B, C, D, E,$ and F, the velocity u reaches a critical maximum u_c and then begins to decrease with increasing u_{SG}. This maximum decreases with increasing magnetic field [Fig. 2(b)]. Figure

2(a), which corresponds to the results obtained by WBK [45] in the case of no dipolar interactions, is also shown here for comparison. The field dependence of u_c is consistent with the result of Nguenang *et al.* [47] as shown in Eq. (2.13).

(iii) In curves G and H of Fig. 2(b), the average velocity decreases gradually down to a value of $u/C_0 = -0.75$ and the initial condition of about $u_{SG}/C_0 = 0.7$, then for the initial condition's velocity greater than $u_{SG}/C_0 = 0.7$, instead of decreasing as in Fig. 2(a), it starts increasing. Such a behavior comes from dipolar effects in the discrete model that creates new nonlinear excitations in the system for high magnetic fields with increasing speed.

Figure 3 illustrates the agreement with Eq. (2.13), and the difference between our result (Fig. 3, curve b) and that of WBK (Fig. 3, curve a). From this we also note that the reduced critical magnetic field is always greater when the dipolar interactions are present (curve b) than when they are absent (curve a). For instance, we have in the static case (i.e., $u=0$) $\hat{b}_c = 0.35$, while $b_c = 0.33$.

Figure 4 presents the curves of the energy in terms of the ratio $\Delta E/E_0$ as a function of the magnetic field for which $\Delta E = E - E_0$, and $E_0 = E$ for $u=0$ is the rest energy of the soliton. A result that appears surprising at a first glance when looking at Fig. 4 is that, by comparing energies for discrete chain with no dipolar interactions (see Fig. 4, curve a) and the case in which dipolar interactions are present (see Fig. 4, curve b), we observe for the curves a and b that the energy decreases gradually with increasing the magnetic field, but while decreasing in the curve b, the energy displays a non-vanishing behavior. However, one must keep in mind that the energy recorded here is that of the maximum mean propagation velocity of the soliton for each field. And that, as shown
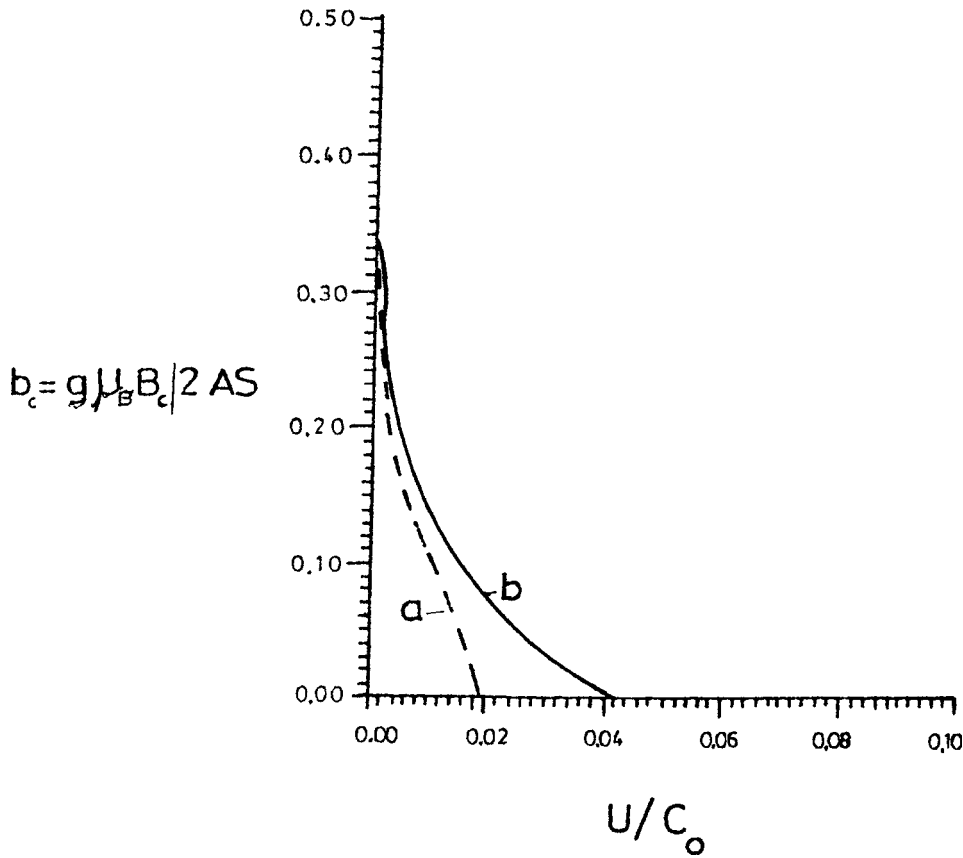
FIG. 3. Maximum mean propagation velocity against magnetic field; curve a is the case without dipolar interactions; curve b is the case with dipolar interactions.

in curve G and H of Fig. 2(b), as the magnetic field is increasing, its combination with dipolar energies in the system finally generates the nonlinear excitations with increasing velocity in the magnetic chain that would increase from their negative values up to the positive one. Since the energy corresponding to positive velocity is greater than E_0, the energy in Fig. 4, curve b, instead of decreasing down to the rest energy E_0 with increasing magnetic field as in Fig. 4, curve a, it decreases down to a minimal value that is greater than the rest energy E_0 of the soliton involving in a magnetic chain without dipolar interactions.

Figure 5 shows the field dependence of the maximum angle of excursion θ_{max}. Figure 5, curve a corresponds to the case of no dipolar interactions, while Fig. 5, curve b illustrates the case with dipolar interactions. The curve a decreases with increasing magnetic field, while the curve b spread out over many extrema leading then to one more stable region than in the case of the curve a. Even in this figure, the curve b (continuous line) clearly indicates the same value of the critical reduced magnetic field $\breve{b}_c = 0.35$, which can be obtained here for the second value of θ_{max} which is nil. Note that here the relative size of H_d with the applied magnetic field is $H_d/B_e \approx 0.0005$ therefore for $s = 1$, $a_1 = 0.001$ [47]. This leads to the value of the critical field obtained from the analytical calculation [see Eq. (2.12)] of $\hat{b}_c \approx 0.37$, which is little bit greater than that of the numerical computation. However, this critical magnetic field is $b_c = \frac{1}{3} \approx 0.33$, for both numerical and analytical calculation when the dipolar interactions are absent.

Figure 6 displays the energy spectrum in terms of the ratio

$\Delta E/E_0$ against mean kink velocity u/C_0 for different magnetic fields.

The results obtained by WBK are shown in Fig. 6(a), while Fig. 6(b) corresponds to the discrete chain in which
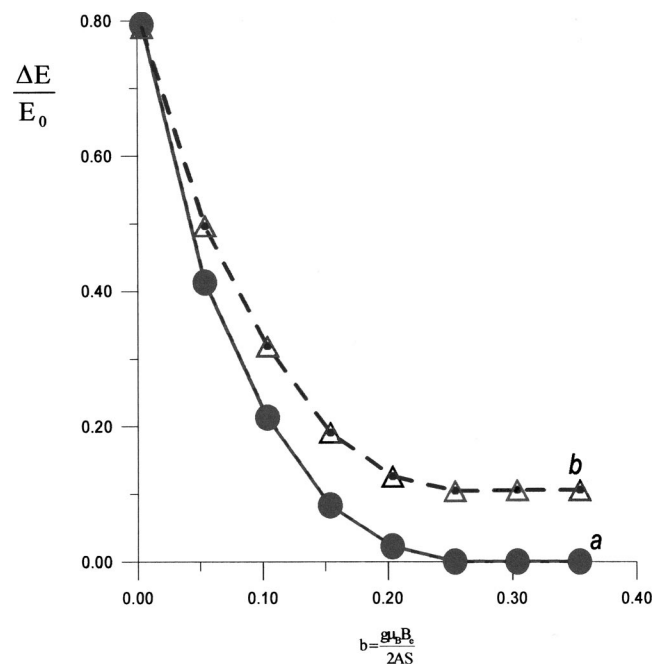

FIG. 4. Energy as function of magnetic field $\Delta E/E_0 = (E/E_0) - 1$; curve a—in the absence of dipolar interaction; curve b—in the presence of dipolar interactions.
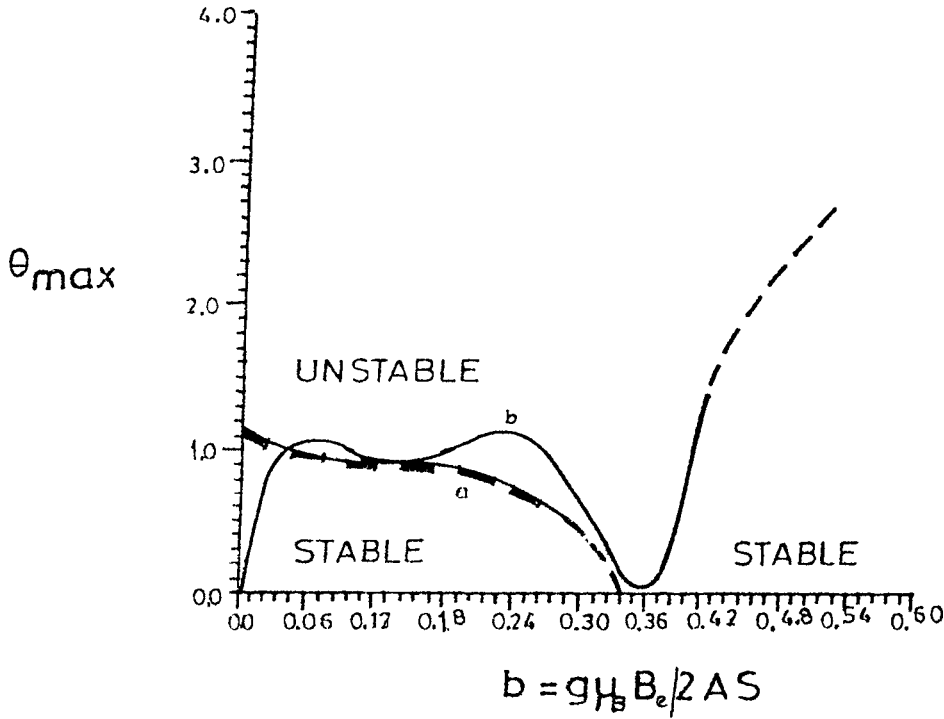
FIG. 5. Stability limit of moving (out-of-plane) soliton in the $\theta_{\max}$, b plane; curve a—in the absence of dipolar interaction; curve b—in the presence of dipolar interactions.

dipolar interactions are taken into account. Figures 6(c) and 6(d) are a zoom that we made from Figs. 6(a) and 6(b), respectively. From these curves one can see that the soliton motion could be classified into five branches according to the size of the out-of-plane angle. Figure 6(d) shows a first branch (I) from point A to B for which the soliton energy increases with its velocity. The energy-velocity relationship along this branch is qualitatively similar to the one given by the perturbed SG equation; therefore this branch is henceforth called the perturbed SG soliton branch. In the branches (II), (III), and (IV), first deviations from the perturbed SG soliton begin to be found and an increase in energy of the solitons results in a decrease of the modulus of their velocity. As pointed out by WBK [45], this first deviation is due to discreteness effect of the spin chain. In the branch (V) [see Fig. 6(d)], the second deviation from the former is found. This is attributed to the discrete dipolar effects. We notice that contrary to the case of Fig. 6(c), the first deviation appears for dynamical soliton instead of a static soliton and there is a new deviation that appears only for high-field values, which can be seen at point D'' in Fig. 6(d). The analytical treatment of this later phenomenon shall be considered in a future publication.

B. Kink-antikink collision

This section presents the results of numerical calculations for classical kink-antikink collision processes in a one-dimensional discrete easy-plane Heisenberg ferromagnet. The results obtained for numerical simulations of a single-soliton dynamics gave valuable qualitative description. Quantitative description needs to simulate kink-antikink head-on collisions at different range of magnetic fields through the discrete equations of motion (2.6) and (2.7). The lattice size is $N=200$, and the parameters of the model have

been chosen so that the kink and antikink width are large with respect to the lattice spacing (typically 10–20 lattice sites) to avoid discreteness effects. Using the same algorithm as for the case of single-soliton dynamics, we also made a numerical analysis of a soliton-antisoliton head-on collision. Only the results of the cases concerned by the introduction of the dipolar interactions shall be presented. The soliton-antisoliton ($S\bar{S}$) pair collision is initiated by starting with a SG $S\bar{S}$ pair that is allowed to evolve in time according to the equations of motion (2.6) and (2.7).

We examine the evolution of an initial condition,

$$\varphi_i = 2\pi - (4\arctan\{\exp[\gamma\sqrt{b}(i-n_1-u_{SG}t)]\}$$
$$+ 4\arctan\{\exp[-\gamma\sqrt{b}(n_2-i+u_{SG}t)]\}), \quad (3.3)$$

$$\theta_i = 2\gamma\sqrt{b}u_{SG}(\text{sech}\{\exp[\gamma\sqrt{b}(i-n_1-u_{SG}t)]\}$$
$$+ \text{sech}\{\exp[-\gamma\sqrt{b}(n_2-i+u_{SG}t)]\}), \quad (3.4)$$

in which the kink and antikink are moving towards each other with the initial velocity u_{SG} which can be interpreted as the input energy. The parameters n_1 and n_2, which are the initial positions of the kink and the antikink at $t=0$, are fixed at appropriate values so that the two solitons do not interfere with each other. Instead of obtaining four major regions as for the case of the ferromagnetic chain with no dipolar interactions, we have obtained here five regions that are summarized as follows.

Region I. The region I is concerned with low applied magnetic fields B_e. The reduced field lies within the range $0\le b\le0.10$. In Figs. 7(a)–7(e), we present a sequence of the time evolutions of a kink-antikink head-on collision for normalized velocities $\nu_1=0.4C_0$ (kink) and $\nu_2=-\nu_1$ (antikink), and for widths equal to $L_1=L_2=10a_0$. In the plot we
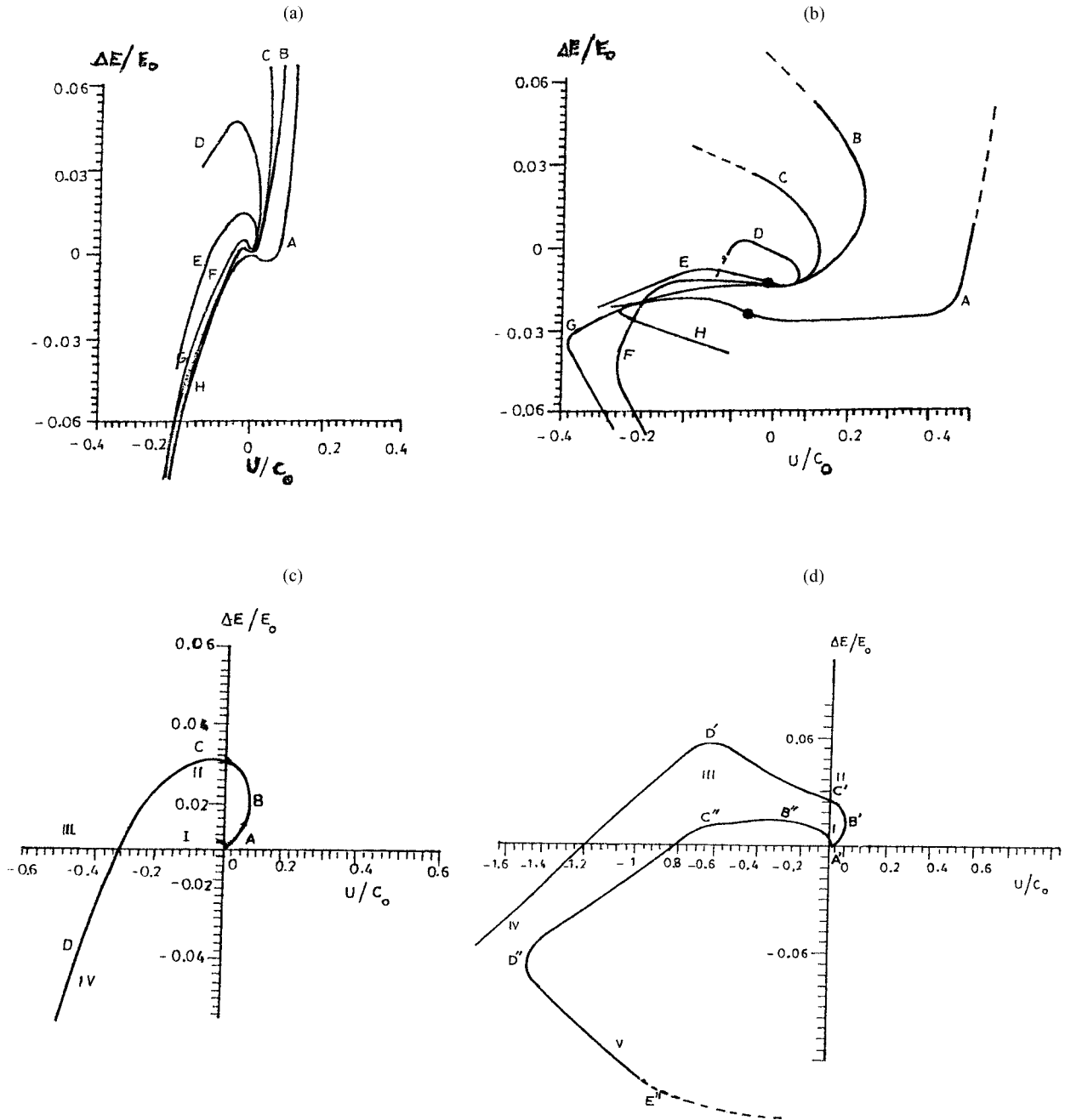
FIG. 6. (a) Discreteness effect on the energy spectrum with mean kink velocity for different reduced magnetic field b; $A=0$, $B=0.05$, $C=0.10$, $D=0.15$, $E=0.19$, $F=0.24$, $G=0.3$, $H=0.36$. When the dipolar interactions are absent. (b) The same figure when the dipolar interactions are present. (c) A zoom in one of the curve of the dispersion curve of (a) in absence of dipolar interactions showing the different regions displayed by the magnetic chain. (d) A zoom in two curves (G and H) of dispersion curve of (b) in presence of dipolar interactions showing the different regions displayed by the magnetic chain. This figure is presented to motivate the physical difference between the two systems.

present the in-plane and out-of-plane components of the spins at different propagation times, and we observed that the collision of a pair of kink-antikink is quasielastic with infinitesimal changes in the soliton forms. The in-plane component of the spin displays a robustness property, whereas the out-of-plane component faces a little distortion of its profile during the collision process. This collision process happens as interpenetration into each other and finally leads to a mutual crossing of both of them. Numerical simulations show

that, even in the presence of dipole-dipole interactions in this range of magnetic field, the solutions of the continuum equations for large width are also good solutions for the discrete medium. Hence, the soliton chosen here as initial condition displays a particlelike behavior. It is also important to note that at normalized low velocity $u_{SG}/C_0 < 0.1$, and mostly in low field, the collision even leads to the formation of a breather, but when the reduced magnetic field is increased to $b=0.08$, it is no longer possible to observe such a phenom-
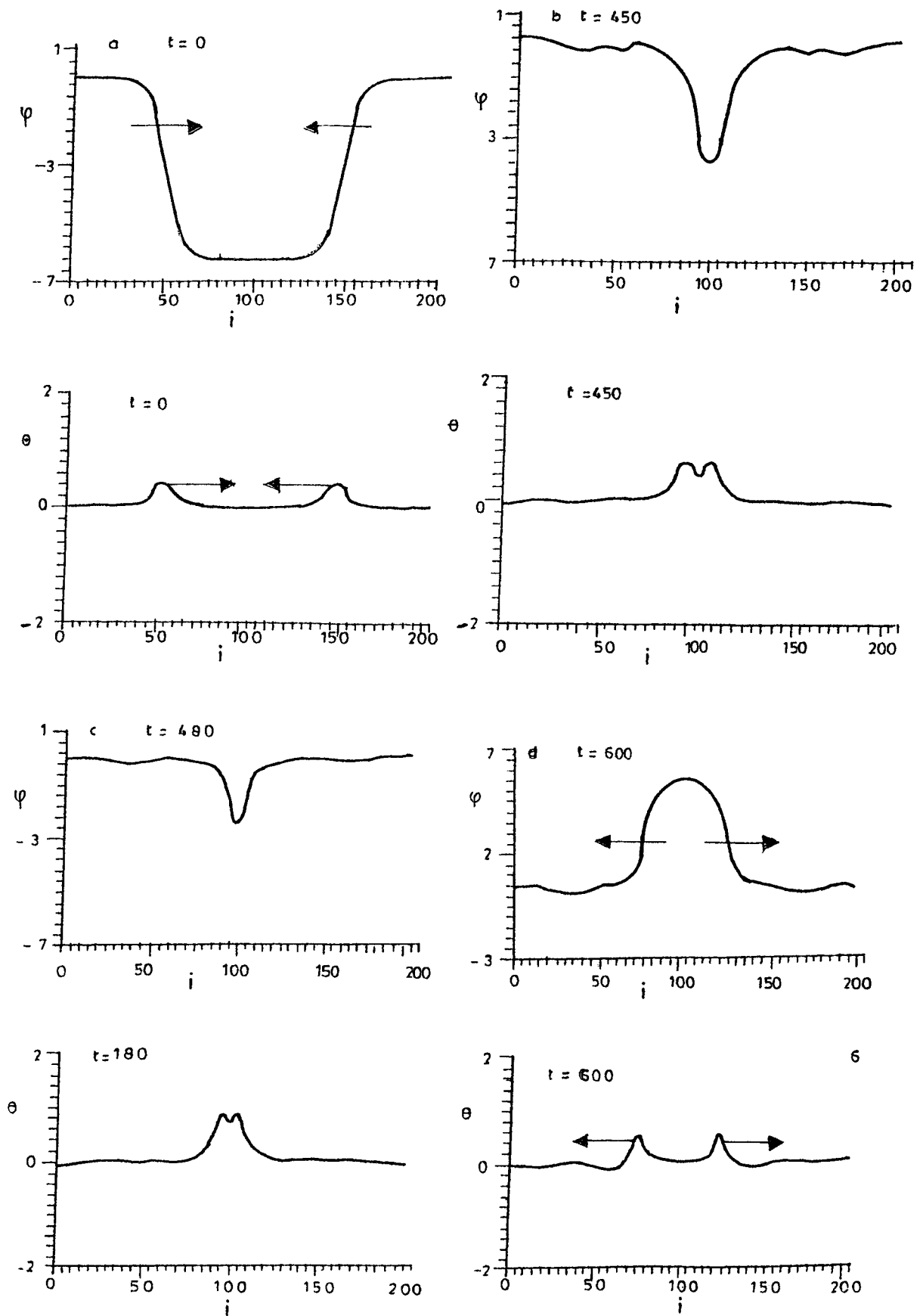
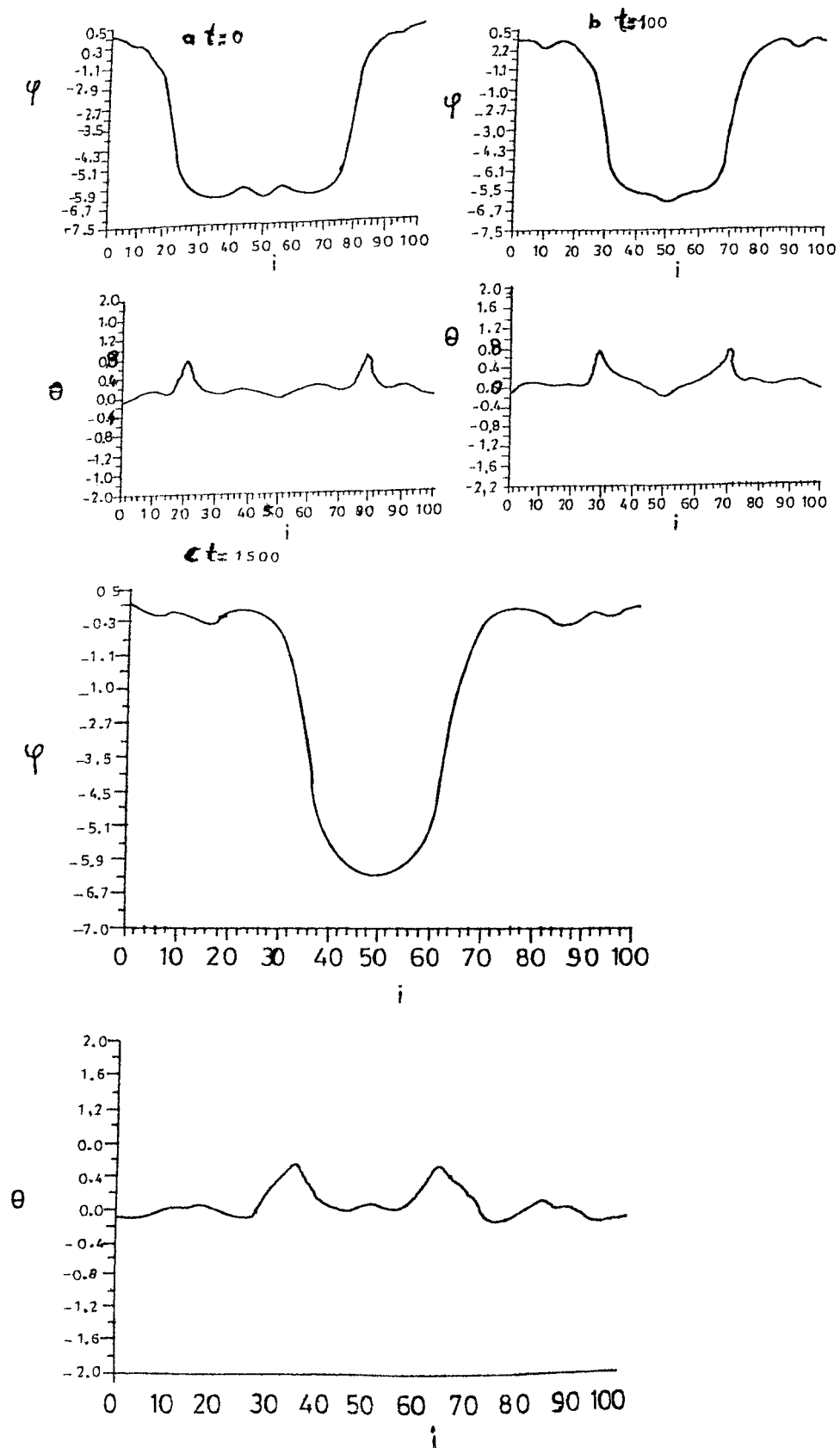FIG. 7. Collisions detail seen at a sequence of times corresponding to region I. $b=0.024$ and $u_{SG}/C_0=0.5$.

FIG. 8. Head-on collision for the region III. $b = 0.16$ and $u_{SG}/C_0 = 0.4$.
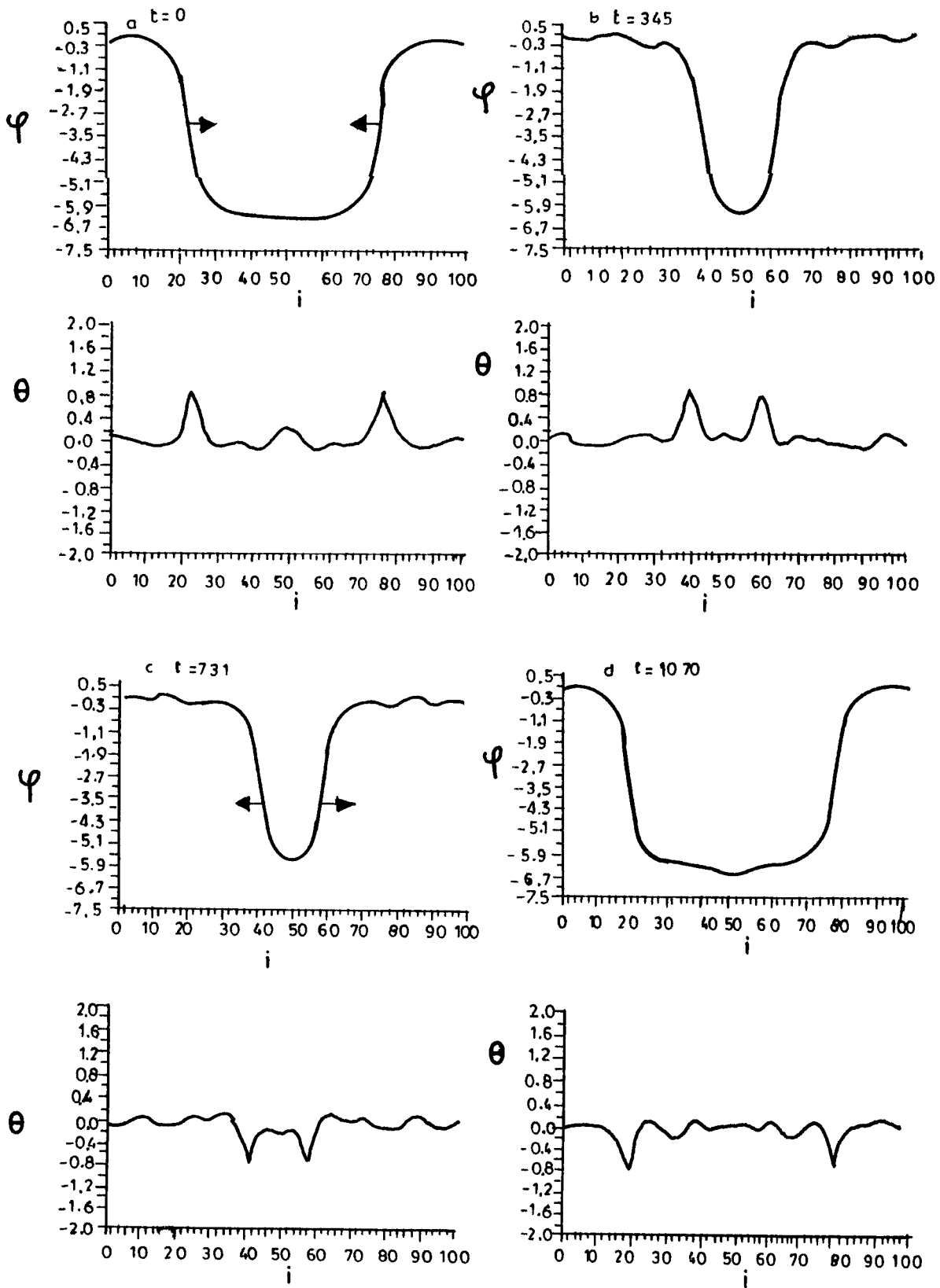
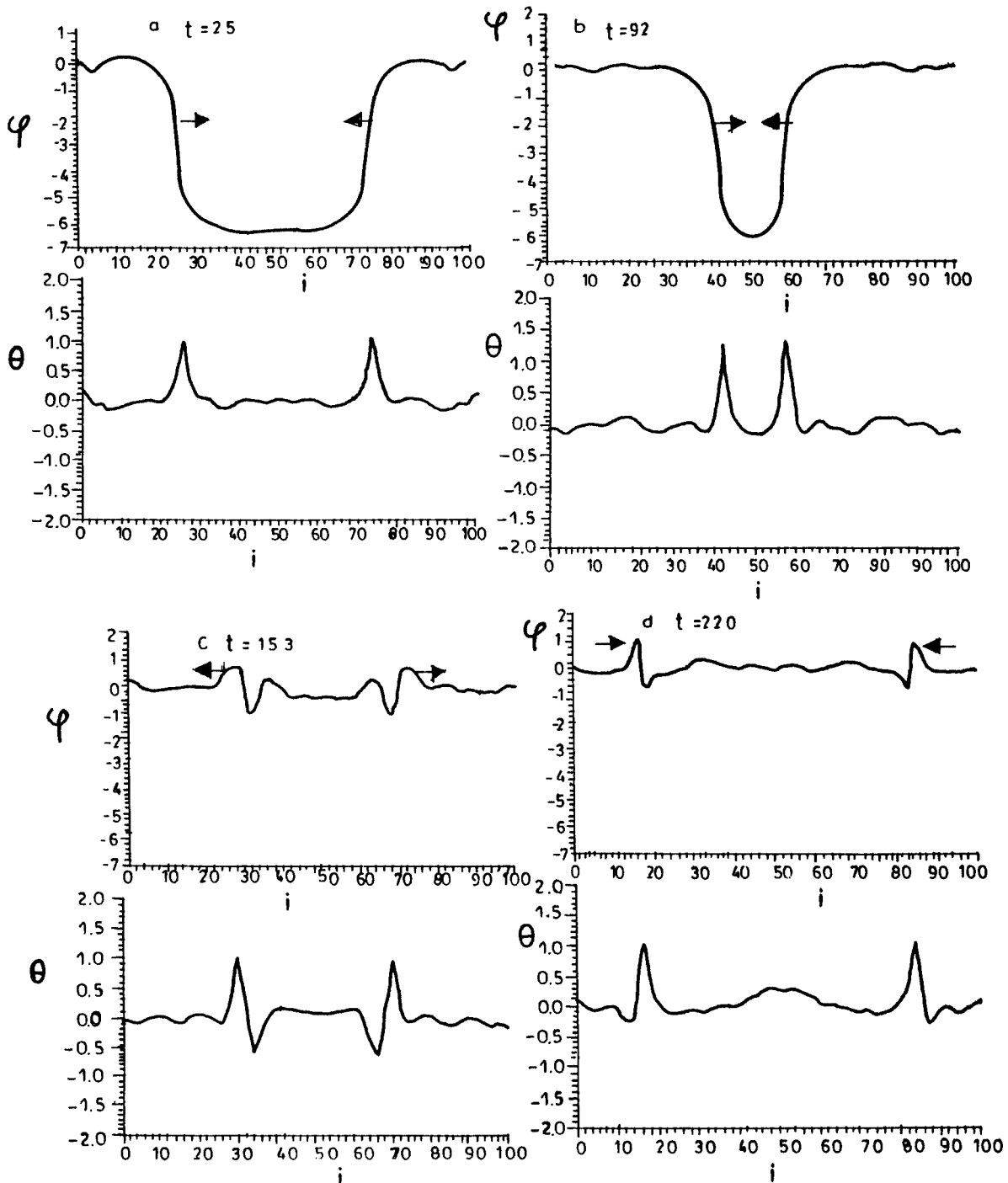FIG. 9. Head-on collision for the region IV. $b = 0.27$ and $u_{SG}/C_0 = 0.4$.

FIG. 10. Head-on collision for a sequence of times for region V. $b=0.37$ and $u_{SG}/C_0=0.45$.

enon for normalized velocities less than 0.1. However, only very high-normalized velocities $u_{SG}/C_0>0.8$ can lead to the breather formation. This breather formation appears as the result of a colliding kink-antikink pair has been interpreted by WBK as a balance of the collision time versus energy dissipation for the kink collective coordinate.

Region II. In this second region, the reduced magnetic field fulfills the following condition: $0.10<b<0.16$. Here, instead of a bound state formation as it is the case when the dipole-dipole interactions are absent [45], the kink-antikink pair is reflected after the collision. This case has been

checked for $b=0.13$ and $u_{SG}/C_0=0.5$, for the external magnetic field and the normalized velocity, respectively, but we will not present the figures here. So, due to periodic boundary conditions, after any collision at the middle of the chain for example, they come out with a velocity of opposite sign and next, they face another collision at the end of the chain. An interesting effect appears for very small-normalized velocity $u_{SG}/C_0 \lesssim 0.1$, where the kink-antikink pair is annihilated after the first collision. This is understandable as the result of the different soliton branches in the chain at very low applied magnetic field.

Region III. In this region, we have $0.16 \leq b < 0.22$. Since the collision time is greater here than those for region II, and I, the size of the chain ranges from 200 to 100. For illustration, we have chosen $b = 0.17$ and the normalized input velocity $u_{SG}/C_0 = 0.3$. In Figs. 8(a)–8(c), we observe that after the collision, there is neither crossing and nor reflection, the system behaves as if it is pinned. In reality, they just stay together and form a pair of kink and antikink. Strictly speaking, such a phenomenon can be observe when the dipolar interactions are absent only in region II for a certain value of the applied magnetic field and velocity [45]. The resulting wave does not display internal oscillation during the simulation and there are only few radiation at the chain ends, we then deduce that, in this range of applied magnetic field, the inclusion of the dipole-dipole interactions in the model leads to a zero frequency translational mode formation.

Region IV. Here, we have $0.22 \leq b \leq 0.32$. The size of the chain is reduced because the collision process is slower than in the case where the dipolar interactions are not included. This is the second region in which we observe the reflection phenomenon after any collision for the in-plane spin component, whereas the out-of-plane component is flipped (see Fig. 9). We also observe some fluctuations on the shapes that come from the scattering effect of the low amplitude magnons that are induced in the system by dipolar interactions. This reflection phenomenon indicates that the soliton of branch II can propagate and survive in this region.

Region V. In this region, the reduced version of the applied magnetic field fulfills $b \geq 0.34$. We observe in Fig. 10 that before the collision, as the soliton waves approach each other, the amplitude of the in-plane spin component φ decreases while that of the out-of-plane θ component increases. After the collision, the in-plane spin component completely changes its shape to behave as a pulse with a flexure slightly oscillating. We deduced that it is a shock wave that comes from a partial restoration process that is induced in the system by the dipole-dipole interactions. In other words, including this long-range magnetic interactions lead us to the fact that, initially from a kink-antikink profile, it follows that the kink and antikink are annihilated through an interpenetrating process. Next, due to a partial restoration process, there appear a pulse shock wave that would continue the collision process without changing. But, the out-of-plane spin component just slightly changes its shape and the initial profile is rapidly reconstructed with greater amplitude.

IV. CONCLUSION

In conclusion, we have analyzed the nonlinear dynamics of the soliton structure taking the model of CsNiF$_3$ material as a particular example, in which the dipole-dipole interactions are taken into account. The different simulations of the soliton's propagation point out that, in the presence of dipolar interactions, when the degree of discreteness is high, the single SG soliton is more likely to fail to provide an appropriate description of the soliton dynamics. We also note from these simulations that, when the degree of discreteness is not to high, the dipolar interactions that are added in the system permitted us to observe that the range of stability is raised

through the critical field and the critical velocity, this can also be observed in the shape of the maximum value of the out-of-plane spin component vs the magnetic field. Thanks to the numerical experiment, the energy against velocity profile presents five region. The new region here leads to the generation of a shock wave that is stable under the collision processes. These dipolar interactions are also responsible for the nonvanishing behavior of the energy of the system with the increasing magnetic field. From the results presented above, it is concluded that the investigation of the dynamics of kink and their collisions comprises an interesting task for physics. Then it may result in a broadening of ordinary understanding of several types of soliton interactions in quasi-one-dimensional system, which are represented by the domain walls of a ferromagnet with uniaxial anisotropy and dipolar interactions.

APPENDIX

In order to find the expression of the constant $A(\lambda)$ in Eq. (2.18), we use the continuum approximation of the discrete system (2.6) and (2.7). In the assumption of small velocities u, we expand the solution in power of u as

$$\theta(s) = u\theta_0(s) + u^3\theta_1(s) + u^5\theta_2(s) + \cdots, \quad (A1)$$

$$\phi(s) = \phi_0(s) + u^2\phi_1(s) + u^4\phi_2(s) + \cdots. \quad (A2)$$

Then to lowest order in u, the continuum system reduced to

$$\frac{d^2\phi_0(s)}{ds^2} - \sin(\phi_0(s)) = 0, \quad (A3)$$

$$-u\frac{d^2\phi_0(s)}{ds^2} = -\frac{d^2\theta_0(s)}{ds^2} + \left[\lambda - \left(\frac{d\phi_0(s)}{ds}\right)^2 + (1+\alpha_1)\cos(\phi_0(s))\right]\theta_0(s), \quad (A4)$$

where $\alpha_1 = 2b_d/b$.
The solution of Eq. (A3) is

$$\phi_0 = 4\arctan(\exp(s)), \quad (A5)$$

with $s = \gamma\sqrt{b}(Z - u_{SG}\tau)$.
By introducing Eq. (A5) into Eq. (A4), Eq. (A4) reduces to

$$(\lambda + \alpha_1 + L_2)\Theta_0(s) = \text{sech}(s), \quad \Theta_0 = -2u\theta_0, \quad (A6)$$

where

$$L_2 = -\frac{d^2}{ds^2} + [1 - 6\,\text{sech}^2(s)]$$

is a Hermitic operator. Here we have neglected the effect of the dipolar field on the diffusion potential. As in Ref. [61], to solve Eq. (A6), we need first to derive the complete orthonormal eigenfunctions $\psi_n(s)$ of

$$L_2 \psi_n = \varepsilon_n \psi_n \tag{A7}$$

as

$$\varepsilon_0 = -3 \quad \text{and} \quad \psi_0(s) = \frac{\sqrt{3}}{2} \text{sech}^2(s), \tag{A8}$$

$$\varepsilon_1 = 0, \quad \text{and} \quad \psi_1(s) = \left(\frac{3}{2}\right)^{1/2} \text{sech}(s)\tanh(s), \tag{A9}$$

$\varepsilon_k = 1 + k^2$ and

$$\psi_k(s) = \frac{\exp(iks)}{\sqrt{(1+k^2)(4+k^2)}}$$
$$\times (1 + k^2 + 3ik\tanh(s) - 3\tanh^2(s)). \tag{A10}$$

Now we can use this complete eigenfunctions to obtain the expression of Θ_0 in Eq. (A6) through a direct approach to the study of soliton perturbation that have been recently used by Yan and Tang [62] to solve a perturbed Korteweg–de Vries equation. For this purpose, we need to assume that both $\Theta_0(s)$ and the right-hand side $[R(s) = \text{sech}(s)]$ of Eq. (A6) should be expanded in a generalized Fourier integral as

$$\Theta_0(s) = \sum_{j=0}^{1} \Theta_0^j \psi_j(s) + P \int_{-\infty}^{+\infty} \Theta_0(k)\psi(s,k)dk, \tag{A11}$$

where

$$\Theta_0(k) = P \int_{-\infty}^{+\infty} \Theta_0(s)\psi(s,k)ds, \tag{A12}$$

where P denotes the principal value of the integral under consideration and the coefficients Θ_0^j are given by

$$\Theta_0^j = \int_{-\infty}^{+\infty} \Theta_0(s)\psi_j(s)ds, \quad j = 0,1. \tag{A13}$$

We also have for the right-hand side of Eq. (A6),

$$R(s) = \sum_{j=0}^{1} R_0^j \psi(s) + P \int_{-\infty}^{+\infty} R_0(k)\psi(s,k)dk, \tag{A14}$$

with

$$R_0(k) = P \int_{-\infty}^{+\infty} R(s)\psi(s,k)ds, \tag{A15}$$

$$R_0^j = \int_{-\infty}^{+\infty} R(s)\psi_j(s)ds, \quad j = 0,1. \tag{A16}$$

Using then Eqs. (A11) and (A14) into Eq. (A6), and note that $L_2\psi_0 = -3\psi_0$, $L_2\psi_1 = 0$, and $L_2\psi_k = (1+k^2)\psi_k$, we then multiply the resulting equation by $\psi(s,k)$, $\psi_0(s)$, and $\psi_1(s)$ successively, and then integrate it over s we obtain the following relations:

$$\Theta_0(k) = \frac{R_0(k)}{1 + \alpha_1 + \lambda + k^2}, \tag{A17}$$

$$\Theta_0^0 = \frac{R_0^0}{\lambda + \alpha_1 - 3}, \quad \Theta_0^1 = \frac{R_0^1}{\lambda}. \tag{A18}$$

Since $R_0^1 = (3/2)^{1/2}\int_{-\infty}^{+\infty} \text{sech}^2(s)\tanh(s)ds = 0$, it implies that $\Theta_0^1 = 0$,

$$R_0^0 = \frac{\sqrt{3}}{2} \int_{-\infty}^{+\infty} \text{sech}^3(s)ds = \frac{\pi\sqrt{3}}{4}. \tag{A19}$$

Then from Eq. (A15)

$$\Theta_0^0 = \frac{\pi\sqrt{3}}{4(\lambda + \alpha_1 - 3)}. \tag{A20}$$

From Eq. (A15), the evaluation of $R_0(k)$ leads to

$$R_0(k) = -\frac{\pi(k^2+1)\text{sech}\left(\dfrac{k\pi}{2}\right)}{2\sqrt{(k^2+1)(k^2+4)}}. \tag{A21}$$

Finally it comes that

$$\Theta_0(s) = \frac{F(s,\lambda)}{\lambda + \alpha_1 - 3}, \tag{A22}$$

where

$$F(s,\lambda) = \frac{3\pi}{8}\text{sech}^2(s) - \frac{3\pi(\lambda + \alpha_1 - 3)}{2} P \int_{-\infty}^{+\infty} \frac{\text{sech}\left(\dfrac{k\pi}{2}\right)\left(\dfrac{k^2+1}{3} + ik\tanh(s) - \tanh^2(s)\right)\exp(iks)}{(k^2+4)(1+\alpha_1+\lambda+k^2)} dk. \tag{A23}$$

Then using the properties of the principal value of an integral with the aid of the residue theorem, Eq. (A23) can be suitably transformed into

$$F(s,\lambda) = \frac{3\pi}{8}\operatorname{sech}^2(s) - \frac{3\pi}{4}\int_{-\infty}^{+\infty} \frac{\operatorname{sech}\left(\frac{k\pi}{2}\right)\left(\frac{\lambda+\alpha_1}{3} - ik\tanh(s) + \tanh^2(s)\right)\exp(iks)}{(1+\alpha_1+\lambda+k^2)}\,dk. \tag{A24}$$

Finally, the expansion of the energy with the velocity leads us to the evaluation of

$$A(\lambda) = \frac{1}{2}\int_{-\infty}^{+\infty} F(s,\lambda)\operatorname{sech}(s)\,ds, \tag{A25}$$

which leads to

$$A(\lambda) = \frac{\pi}{4}\left[\frac{3\pi}{4} + \frac{\lambda+\alpha_1}{2\sqrt{1+\alpha_1+\lambda}}\,\psi'\left(\frac{1+\sqrt{1+\alpha_1+\lambda}}{2}\right)\right], \tag{A26}$$

where ψ' is the digamma function.

---

[1] R. K. Dodd, J. C. Eilbeck, J. D. Gibbon, and H. C. Morris, *Solitons and Nonlinear Wave Equations* (Academic, London, 1982).

[2] F. Nabarro, *Theory of Crystal Dislocations* (Clarendon, Oxford, 1967).

[3] M. Remoissenet, *Waves called Solitons, Concepts, and Experiments*, 3rd ed. (Springer, New York, 1999).

[4] M. Peyrard and M. D. Kruskal, Physica D **14**, 88 (1984).

[5] C. R. Willis, M. El-Batanouny, and P. Stancioff, Phys. Rev. B **33**, 1904 (1986).

[6] R. Boesch and C. R. Willis, Phys. Rev. B **39**, 361 (1989).

[7] O. Bang and M. Peyrard, Physica D **81**, 9 (1995).

[8] P. Woafo, T. C. Kofané, and A. S. Bokosah, Phys. Rev. B **48**, 10 153 (1993).

[9] M. Peyrard, St. Pnevmatikos, and N. Flytzanis, Physica D **19**, 268 (1986).

[10] C. R. Willis and R. Boesch, Phys. Rev. B **41**, 4570 (1990).

[11] P. Woafo, T. C. Kofané, and A. S. Bokosah, J. Phys.: Condens. Matter **4**, 3389 (1992).

[12] C. M. Ngabireng and T. C. Kofané, Phys. Scr. **55**, 257 (1997).

[13] D. Yémélé and T. C. Kofané, Phys. Rev. B **56**, 3353 (1997).

[14] D. N. Christodoulides and R. I. Joseph, Opt. Lett. **13**, 794 (1988).

[15] Y. S. Kivshar and M. Peyrard, Phys. Rev. A **46**, 3198 (1992).

[16] S. Darmanyan, I. Relke, and F. Lederer, Phys. Rev. E **55**, 7662 (1997).

[17] O. Bang, J. J. Rasmissen, and P. L. Christiansen, Nonlinearity **7**, 205 (1993).

[18] E. W. Laedke, K. H. Spatschek, and S. K. Turitsyn, Phys. Rev. Lett. **73**, 1055 (1994).

[19] A. J. Sievers and S. Takeno, Phys. Rev. Lett. **61**, 970 (1988).

[20] S. Takeno, K. Kisoda, and A. J. Sievers, Prog. Theor. Phys. Suppl. **94**, 242 (1988).

[21] V. M. Burlakov, S. A. Kiselev, and V. N. Pyrkov, Phys. Rev. B **42**, 4921 (1990).

[22] S. Grossmann and H. Fujisaka, Phys. Rev. A **26**, 1779 (1982).

[23] Kivshar, Phys. Rev. Lett. **70**, 3055 (1993).

[24] Huang and Z. Jia, Phys. Rev. B **51**, 613 (1995).

[25] C. Schmidt-Hattenberger, U. Trustschel, and F. Lederer, Opt. Lett. **16**, 294 (1991).

[26] C. Schmidt-Hattenberger, R. Muschall, F. Lederer, and U. Trustschel, J. Opt. Soc. Am. B **10**, 1592 (1993).

[27] P. E. Langridge and W. J. Firth, Opt. Quantum Electron. **24**, 1315 (1992).

[28] M. I. Molina and G. P. Tsironis, Physica D **65**, 267 (1993).

[29] A. V. Aceves, C. De Angelis, A. M. Rubenchik, and S. K. Turitsyn, Opt. Lett. **19**, 329 (1994).

[30] A. S. Davydov, *Solitons in Molecular Systems* (Reidel, Dordrecht, 1987).

[31] P. L. Christiansen, O. Bang, S. Pagano, and G. Vitiello, Nanobiology **1**, 229 (1992).

[32] P. Marquié, J. M. Bilbault, and M. Remoissenet, Phys. Rev. E **51**, 6127 (1995).

[33] B. Z. Essimbi, A. A. Zibi, A. Zamé, and T. C. Kofané, J. Phys. Soc. Jpn. **64**, 2777 (1995).

[34] B. Z. Essimbi, L. Ambassa, and T. C. Kofané, Physica D **106**, 207 (1997).

[35] T. Dauxois and M. Peyrard, Phys. Rev. Lett. **70**, 3935 (1993).

[36] M. Peyrard and A. R. Bishop, Phys. Rev. Lett. **62**, 2755 (1989).

[37] T. Dauxois, M. Peyrard, and A. R. Bishop, Phys. Rev. E **47**, 684 (1993).

[38] T. Dauxois, M. Peyrard, and A. R. Bishop, Phys. Rev. E **47**, R44 (1993).

[39] T. Erneux and G. Nicolis, Physica D **67**, 237 (1993).

[40] J. P. Keener, J. Theor. Biol. **148**, 49 (1991).

[41] J. Bell, in *Reaction-Diffusion Equations*, edited by K. J. Brown and A. A. Larey (Clarendon, Oxford, 1990), pp. 95–116.

[42] D. Takahashi and J. Matsukidaira, Phys. Lett. A **209**, 184 (1995).

[43] R. Roncaglia and G. P. Tsironis, Phys. Rev. Lett. **81**, 10 (1998).

[44] G. M. Wysin, A. R. Bishop, and P. Kumar, J. Phys. C **15**, L337 (1982).

[45] G. M. Wysin, A. R. Bishop, and P. Kumar, J. Phys. C **17**, 5975 (1984).

[46] S. Roche and M. Peyrard, Phys. Lett. A **172**, 236 (1993).

[47] J. P. Nguenang, T. C. Kofané, E. Yomba, and J. D. Yo, Phys. Scr. **60**, 460 (1999).

[48] R. Ferrer, Physica B & C **132**, 56 (1985).

[49] J. Adler, Ph.D. thesis, University of New South Wales, 1979 (unpublished).

[50] P. W. Anderson, Phys. Rev. **15**, 2 (1959).

[51] D. V. Kapor and M. J. Skrinjar, Europhys. Lett. **3**, 953 (1987).

[52] S. Ma and G. F. Mazenko, Phys. Rev. B **11**, 4077 (1975).

[53] A. Aharony, Phys. Rev. B **8**, 3342 (1973).

[54] C. Etrich, H. J. Mikeska, E. Magyari, H. Thomas, and R. Weber, Z. Phys. B: Condens. Matter **62**, 97 (1985).

[55] R. Ferrer, A. Hamed, and F. Lund, Phys. Rev. B **33**, 1752 (1986).

[56] H. J. Mikeska, J. Phys. C **11**, L29 (1978).

[57] P. Kumar, Phys. Rev. B **25**, 483 (1982).

[58] P. Kumar, Physica D **5**, 359 (1982).

[59] E. Magyari and H. Thomas, Phys. Rev. B **25**, 532 (1982).

[60] R. Liebmann, M. Schöbinger, and D. Hackenbracht, J. Phys. C **16**, L633 (1983).

[61] L. D. Landau and E. M. Lifshitz, *Quantum Mechanics* (Pergamon, New York, 1959), pp. 69–70.

[62] J. Yan and Y. Tang, Phys. Rev. E **54**, 6816 (1996).